Ultrasonics Sonochemistry 74 (2021) 105557

Contents lists available at ScienceDirect

Ultrasonics Sonochemistry

journal homepage: www.elsevier.com/locate/ultson

One-step synthesis of black TiO_{2-x} microspheres by ultrasonic spray pyrolysis process and their visible-light-driven photocatalytic activities

Myeongjun Ji [a], Yong-Ho Choa [c], Young-In Lee [a,b,*]

[a] Department of Materials Science and Engineering, Seoul National University of Science and Technology, Seoul 01811, Republic of Korea
[b] The Institute of Powder Technology, Seoul National University of Science and Technology, Seoul 01811, Republic of Korea
[c] Department of Materials Science and Chemical Engineering, Hanyang University, Ansan-si 15588, Republic of Korea

ARTICLE INFO

Keywords:
Microsphere
Photocatalyst
Black TiO_{2-x}
Ultrasonic spray pyrolysis
Photodegradation

ABSTRACT

Black TiO_{2-x} has recently emerged as one of the most promising visible-light-driven photocatalysts, but current synthesis routes that require a reduction step are not compatible with cost-effective mass production and a relatively large particle such as microspheres. Herein, we demonstrate a simple, fast, cost-effective and scalable one-step process based on an ultrasonic spray pyrolysis for the synthesis of black TiO_{2-x} microspheres. The process utilizes an oxygen-deficient environment during the pyrolysis of titanium precursors to directly introduce oxygen vacancies into synthesized TiO_2 products, and thus a reduction step is not required. Droplets of a titanium precursor solution were generated by ultrasound energy and dragged with continuous N_2 flow into a furnace for the decomposition of the precursor and crystallization to TiO_2 and through such a process spherical black TiO_{2-x} microspheres were obtained at 900 °C. The synthesized black TiO_{2-x} microsphere with trivalent titanium/oxygen vacancy clearly showed the variation of physicochemical properties compared with those of white TiO_2. In addition, the synthesized microspheres presented the superior photocatalytic activity for degradation of methylene blue under visible light irradiation. This work presents a new methodology for a simple one-step synthesis of black metal oxides microspheres with oxygen vacancies for visible-light-driven photocatalysts with a higher efficiency.

1. Introduction

In recent years, energy shortages and environmental pollution have emerged as the most important problems mankind has to tackle. As one of the prospective technologies, semiconductor photocatalysis plays a considerable role for generating hydrogen and oxygen from water, inactivating viruses and/or completely eliminating the broad range of organic pollutants under the illumination of sunlight under ambient conditions [1–4]. Among all semiconductor photocatalytic materials, titanium dioxide (TiO_2) has been extensively investigated as a photocatalyst for environmental cleanup, solar cells, clean H_2 energy production, and antimicrobial activity due to its favorable band-edge positions, strong optical absorption and superior characteristics, such as nontoxicity, chemical stability, highly photocatalytic activity, and environmentally friendly [4–6]. However, due to its wide band-gap of 3.2 eV, TiO_2 can only be excited by ultraviolet or near-ultraviolet radiation (200–400 nm) of incoming sunlight on the earth which contain major portion as 43% visible (400–700 nm) and 52% IR (700–2500 nm) radiation energy. Therefore, it is of top priority to develop visible-light-driven (VLD) photocatalysts which can increase the absorption. There are many different approaches and attempts to address this intrinsic limitation of TiO_2 by doping with various metal and non-metal atoms, depositing or decorating the surface of TiO_2 nanostructures by noble metal nanoparticles and constructing heterojunctions with other semiconducting materials [7–9].

The recent discovery of black TiO_2 nanoparticles by Mao and coworkers in 2011 has triggered an explosion of interest and opened a new approach to boost the full spectrum sunlight absorption for an enhanced photocatalytic performance [10]. The black TiO_2 is featured by self-structural modifications, involving self-doped Ti^{3+}/oxygen vacancy, or incorporation of H-doping [10,11]. Due to these modifications, not only the surface properties but also the crystal and electronic structure change greatly, and the most noticeable effect is the color change. After the pioneer work by Mao, the study on the new synthetic approaches of

* Corresponding author at: Department of Materials Science and Engineering, Seoul National University of Science and Technology, Seoul 01811, Republic of Korea.
E-mail address: youngin@seoultech.ac.kr (Y.-I. Lee).

https://doi.org/10.1016/j.ultsonch.2021.105557
Received 24 December 2020; Received in revised form 6 April 2021; Accepted 12 April 2021
Available online 15 April 2021

black TiO_2 has been actively conducted to investigate the structure and properties relationship of black TiO_2 and to utilize it to various functional applications [10–13]. To date, thermal treatment approaches of white TiO_2 in reducing atmosphere such as H_2, H_2/Ar and H_2/N_2 or with metals such as Al, Zn and Mg are the widely used method to synthesize the black TiO_2 [10–15]. However, the reduction based methods have some major drawbacks such as the need for high temperature or a high pressure, a prolonged reaction time and sophisticated environment. Above all, it should not be overlooked that the reduction-based method requires the synthesis of white TiO_2 in advance, and the applicable particle size is limited to the nanoscale level. In practical photocatalytic applications, TiO_2 microsphere photocatalysts can be better than corresponding nanoparticles because the nanoscale materials often suffer from deactivation, agglomeration and precipitation for photocatalyst recycling after the initial run.

In the present work, we demonstrate a simple and facile one-step synthesis of black TiO_{2-x} microsphere with oxygen vacancies and Ti^{3+} interstitial defects using a simple, low-cost and scalable ultrasonic spray pyrolysis (USP) process. The major concept is that utilizing an oxygen-deficient environment during the decomposition and crystallization of titanium precursor micro-droplets generated by ultrasound energy to directly introduce oxygen vacancies into synthesized TiO_2 products. To best of our knowledge, this is the first time that the one-step direct synthesis of black TiO_{2-x} microspheres using the USP process is reported. The physicochemical properties of as-synthesized particles were analyzed by various tools and compared with its white form. Furthermore, the photocatalytic activity of the black TiO_{2-x} has been evaluated using the degradation of methylene blue under visible light irradiation.

2. Experimental details

Starting precursor solutions for the USP were prepared by dissolving titanium (IV) isopropoxide (TTIP, $Ti(C_3H_7O)_4$, 99.9%, Sigma-Aldrich) with the concentration of 100 mM in anhydrous ethanol under vigorous stirring for 60 min. For the USP process, the precursor solution is ultrasonically atomized by an ultrasonic mist generator (1.7 MHz of frequency) into microdroplets. They were carried by a N_2 gas flow (flow rate of 2 L/min) into a tube furnace, and then thermally pyrolyzed through the heating stage in N_2 currents at 900 °C which is black in color as shown in Fig. 1. A subsequent thermal treatment of the powder synthesized at 900 °C was performed at 500 °C in air for 1 h to transform the black sample to a white powder (Fig. 1) for comparing physicochemical, optical and photocatalytic properties. The black and white samples were named BTM-900 and WTM-900, respectively.

Morphological and crystallographic characterizations of the synthesized products were performed by using field emission scanning electron microscopy (FE-SEM, S-4800, Hitachi, Japan) and X-ray diffractometer (XRD, X'Pert3 Powder, PANalytical, Netherlands). Raman spectra were obtained using a LabRAM HR spectrometer (HORIBA Jobin Yvon, France). The specific surface area of the powders was determined using the Brunauer-Emmett-Teller (BET) method from the N_2 adsorption isotherm. Chemical compositions and states were analyzed using X-ray photoelectron spectroscopy (XPS, K-Alpha+, Thermo Fisher Scientific, United States). The UV–vis and diffuse reflectance (DR) spectra were recorded on a UV–vis spectrophotometer (SHIMADZU UV-2600, SHIMADZU Japan) equipped with an integration sphere, using $BaSO_4$ as a reference. The behavior of the photoexcited charge carriers was investigated by photoluminescence (Fluorolog3 with TCSPC, HORIBA Scientific, Japan) with an excitation wavelength of 316 nm.

The visible-light-driven photocatalytic activities of the microspheres were evaluated by measuring the photodegradation rate of methylene blue (MB). This experiment was carried out by adding 0.10 g of microspheres to 100 mL of 2×10^{-5} M MB aqueous solution. The mixture was kept in the dark for 30 min to reach their adsorption–desorption equilibrium. The photodegradation test was performed using a solar simulator equipped with a 300 W xenon lamp and Air Mass 1.5 Global Filter. For those runs performed under visible light, a filter with a 395 nm cut-off was employed (Newport FSQ-GG395, 50.8 mm × 50.8 mm). A series of certain volumes of samples were withdrawn at 30 min intervals for analysis. After centrifugation at 9000 rpm for 5 min, the residual concentration of MB in each sample was determined by the UV/Vis spectrophotometer (UV-2600, Shimadzu, Japan). The absorption spectra of MB were obtained from 500 nm to 750 nm at an interval of 0.3 nm. The photocatalytic mechanism experiments were conducted in identical conditions to further investigate the major reactive species

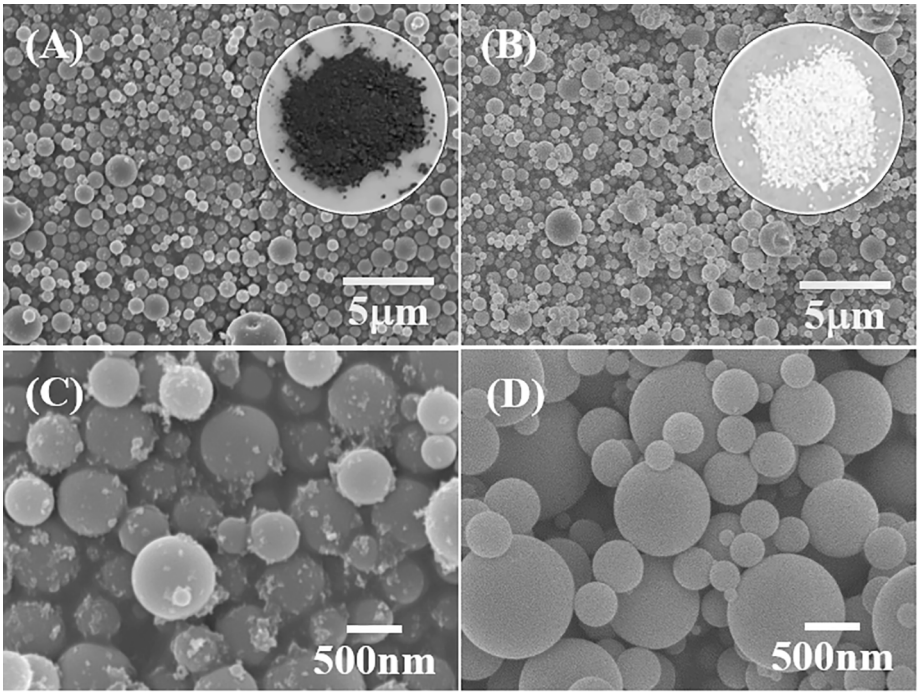

Fig. 1. FE-SEM micrographs and optical photographs of the (a,b) BTM-900 and (c,d) WTM-900.

using the 0.02 mM of triethanolamine (TEOA), *tert*-butanol (TB), and benzoquinone (BQ) as scavengers of h^+, ·OH, and $\cdot O_2^-$, respectively.

3. Results and discussion

FE-SEM micrographs and optical photographs of the BTM-900 and WTM-900 are depicted in Fig. 1. In general, the powder prepared by a typical USP process shows a spherical morphology with a sub-micron or a few micron sizes due to the shape and size of ultrasonically generated initial droplets. The FE-SEM images reveal that BTM-900 is an isotropic sphere with a relatively broad size distribution. After subsequent calcination for a decrease in oxygen vacancies of the BTM-900, their surface became smoother than BTM-900, but size distributions did not change. In order to investigate the surface area, the N_2 adsorption–desorption isotherm curves of both samples, presented in Fig. S1(a), can be classified as type IV in the IUPAC classification with a distinct hysteresis loop in the range of 0.4–1.0 P/P_0, indicating the characteristic of porous material. The BET specific surface area of the BTM-900 and WTM-900 is 10.56 m^2/g and 4.57 m^2/g, respectively. From the Barrett-Joyner-Halenda (BJH) pore-size distribution, Fig. S1(b), it is clear that BTM-900 has a large number of pores in the mesopore range compared to WTM-900 due to its relatively rough surface. In addition, both BTM-900 and WTM-900 exhibited typical XRD patterns of anatase (JCPDS# 21–1272) and rutile (JCPDS# 21–1276) TiO_2 without any additional diffraction peaks as shown in Fig. S2, indicating there was no detectable phase change by the calcination treatment. However, the full width at half maximum of the WTM-900 was slightly smaller than that of BTM-900, whereas the peak intensity was higher than that of BTM-900. This clearly shows the increase in crystallinity due to the decrease in oxygen vacancies by the subsequent calcination treatment [16,17].

Although their morphology and phase were the same, their color was markedly different as shown in the inset images of Fig. 1. The BTM-900 prepared by USP showed a black color but the WTM-900 obtained by thermally treating the BTM-900 in air was white in color. This difference in color shows the presence or absence of oxygen vacancies well and the formation mechanism of oxygen-deficient TiO_{2-x} through the USP process can be proposed as follow. An ethanol used as solvent is decomposed to ethyl group and water above its decomposition temperature. A TTIP [$Ti(OR)_4$], a precursor of titanium, can be converted into $Ti(OR)_2(OH)_2$ by reacting with the generated water. Thereafter, TiO_2, H_2O and ROH are formed during the pyrolysis $Ti(OR)_2(OH)_2$ [18]. In addition, it is well known that the ethyl group (C_2H_5) in ethanol and isopropyl group (C_3H_6) in the TTIP can readily react with oxygen, through which they form CO_2 and H_2O. Therefore, the ethyl and isopropyl group generated by the thermal decomposition of ultrasonically sprayed TTIP/ethanol droplets can lead to oxygen vacancies and/or Ti^{3+} defects in the final TiO_2 microspheres by reacting with the oxygen atoms constituting TiO_2 to form CO_2 and H_2O during the crystallization process of TiO_2. The generated defects are responsible for the formation of mid-gap states resulting in improving light absorption in the visible light region, and as a result, the BTM-900 sample appears black [10,11]. The subsequent heat treatment of the BTM-900 in an oxygen atmosphere can remove the defects and the sample's color changes from black to white (WTM-900) which is the natural color of TiO_2.

The presence and absence of Ti^{3+} and oxygen vacancies were determined by Raman spectroscopy and XPS. Fig. 2(a) shows the Raman spectra of both BTM-900 and WTM-900 microspheres. They exhibited similar five active modes at approximately 148 cm^{-1} (E_g), 201 cm^{-1} (E_g), 399 cm^{-1} (B_{1g}), 518 cm^{-1} (A_{1g}), and 640 cm^{-1} (E_g) which corresponded with those of anatase TiO_2 in the literatures [13,19]. For the BTM-900 microsphere, Most of the peaks widened and weakened compared to the WTM-900. Also, the strongest E_g mode area at 148 cm^{-1} exhibits a blue shift and the peak at 201 cm^{-1} became relatively clear. As reported in the previous studies, these changes were associated with the disorder and non-stoichiometry in the TiO_2 crystal that originated from the oxygen vacancies [13,16,19]. The chemical states of BTM-900 and WTM-900 were determined by XPS. Fig. 2(b) were depicted the two peaks centered at 458.4 eV (Ti $2p_{3/2}$) and 464.0 eV (Ti $2p_{1/2}$) which were characteristic of Ti^{4+} in TiO_2 [20]. Additional peak was observed at 456.4 eV which is assigned to Ti^{3+} [21,22]. The area ratios of Ti^{3+} to Ti $2p_{1/2}$ are 0.13 and 0.06 for BTM-900 and WTM-900 samples, respectively, indicating a larger Ti^{3+} state density in BTM-900. Fig. 2(c) shows the O 1 s state with two overlapping peaks. The peaks at 530.1 eV and 532.1 eV were attributed to lattice oxygen in TiO_2 and oxygen vacancies, respectively [22–24]. The BTM-900 showed the peak at 532.1 eV with a significantly higher intensity than WTM-900. From these results, it was confirmed that there is a higher density of oxygen vacancies in BTM-900.

Fig. 3(a) shows the UV–vis/DR spectra of the microspheres. The UV–Vis spectrum of the WTM-900 showed typical absorption of TiO_2, whereas the BTM-900 showed distinct absorption in the visible region due to the formation of mid-gap states by the defects and these results are consistent with previous studies [13,25–28]. The band gap energies were calculated by a plot of $(ah\nu)^2$ vs energy ($h\nu$) using a Butler equation of $(\alpha h\nu)^2 = A(h\nu - E_g)$ [30]. As shown in Fig. S3, the band gap of the WTM-900 was 3.05 eV. On the other hand, the BTM-900 displayed two-part of the slope, in which the relatively small band gap energy of 2.82 eV is ascribed to the intermediate band formed below the conduction band and the large band gap of 3.22 eV is attributed to the intrinsic band gap of TiO_2 [25,31–33]. The photoluminescence (PL) spectrum of BTM-900, shown in Fig. 3(b), exhibited a slight shift into longer wavelength compared to WTM-900, indicating the increase of the emission from the mid-gap states [13,25]. Moreover, the lower intensity indicates the efficient carrier separation due to trap states induced by the defects [29,35]. These differences resulted from the oxygen vacancies and Ti^{3+} defects in the BTM-900 indicate the possibility for photocatalytic activity driven by visible light of BTM-900. The MB catalytic degradation rate by the BTM-900 and WTM-900 was evaluated by confirming C/C_0 changes over reaction time and was assigned to a pseudo-first-order kinetics reaction with a simplified Langmuir–Hinshelwood model

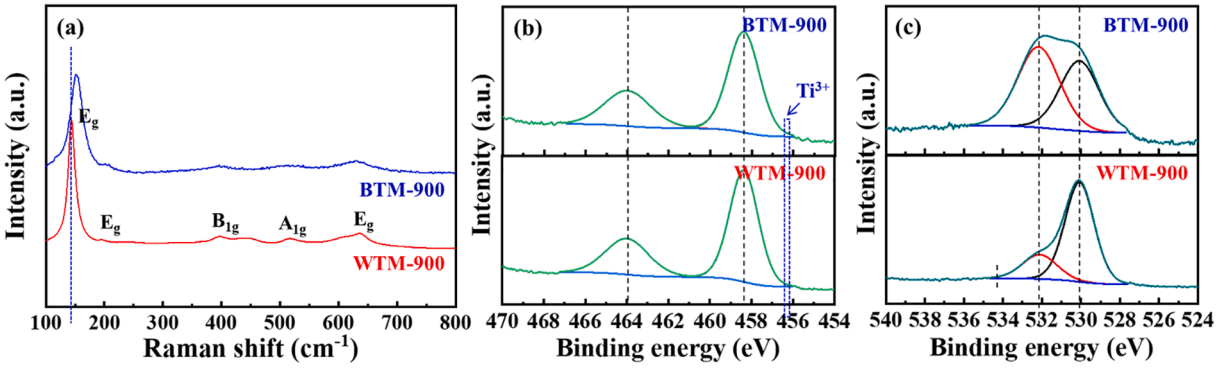

Fig. 2. (a) Raman scattering spectra and XPS spectra of (b) Ti 2p and (c) O 1 s of BTM-900 and WTM-900.

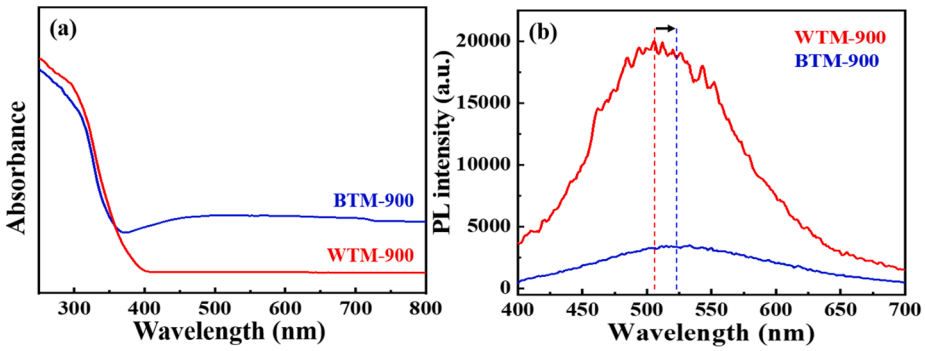

Fig. 3. (a) The UV–vis/DR absorption spectra and (b) the photoluminescence (PL) spectra of BTM-900 and WTM-900.

[34]. As shown in Fig. 4, the BTM-900 with a higher density of Ti^{3+} and oxygen vacancies shows the better photocatalytic degradation efficiency than the WTM-900 and the apparent rate constant k of the BTM-900 is 0.01040, which is 22.1 times of that over WTM-900 sample (k = 0.00047). Although the adsorption capacity of the BTM-900 was higher than WTM-900 due to the synergistic effect between relatively large surface area and introduced defects, before the photocatalytic experiment, an adsorption–desorption equilibrium was achieved in the dark-room as shown in Fig. S4. Therefore, it can be concluded that the removal of MB under visible light irradiation is only attributed to photocatalysis, not adsorption. These results show that the introduction of Ti^{3+} and oxygen vacancies into the TiO_2 microspheres can significantly improve the photocatalytic activity of visible light irradiation and consistent with the previous studies [35–37].

The photocatalytic mechanism experiments were conducted using different radical scavenger under identical conditions and the results are shown in Fig. 5. In general, the photocatalytic mechanism of TiO_2 can be explained by the reaction equation (1)–(9) as follow: [38,39]

$$TiO_2 + h\nu \rightarrow h^+_{vb} + e^-_{cb} \quad (1)$$

$$e^-_{cb} + O_2 \rightarrow \cdot O_2^- \quad (2)$$

$$\cdot O_2^- + H^+ \rightarrow \cdot HO_2 \quad (3)$$

$$\cdot HO_2 + \cdot HO_2 \rightarrow H_2O_2 + O_2 \quad (4)$$

$$e^-_{cb} + H_2O_2 \rightarrow \cdot OH + OH^- \quad (5)$$

$$h^+_{vb} + OH^- \rightarrow \cdot OH \quad (6)$$

$$h^+_{vb} + H_2O \rightarrow H^+ + \cdot OH \quad (7)$$

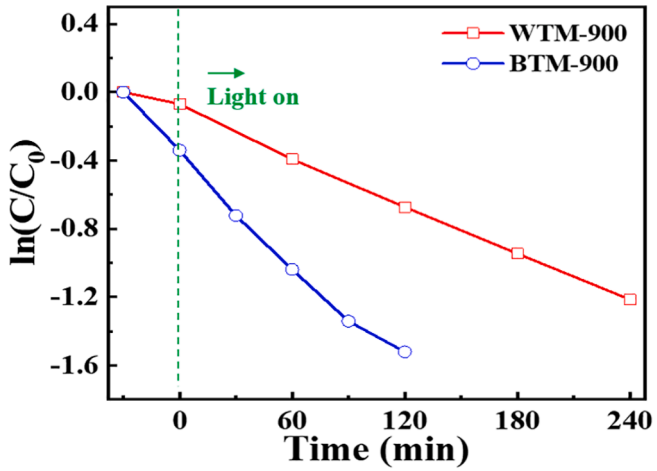

Fig. 4. kinetics of the photocatalytic degradation of MB assigned to a pseudo-first-order transforms $\ln(C/C_0) = kt$ for BTM-900 and WTM-900.

$$Dye + \cdot O_2^- \rightarrow OX\ prod \quad (8)$$

$$Dye + \cdot OH \rightarrow OX\ prod \quad (9)$$

At the beginning, photoexcited electrons and holes separate and migrate to the surface of TiO_2. Then the electrons are reacted with dissolved O_2 in the dyes solutions to produce superoxide radicals ($\cdot O_2^-$). These radicals can directly oxidize dyes. Moreover, because H_2O_2 is a good electron acceptor, the photoexcited electrons can be captured by H_2O_2 which is produced by a continuous reaction from $\cdot O_2^-$, following on converting into hydroxyl radicals ($\cdot OH$) to oxidize dyes. On the other hand, the photogenerated holes can be trapped by hydroxyl ions or H_2O molecules to form $\cdot OH$. Therefore, the dye molecules can be oxidized by $\cdot OH$ and O^{2-} and then decomposed to nontoxic smaller molecules. The reduction in efficiency by scavengers, shown in Fig. 5, obviously exhibited the generation of reactive oxygen species by BTM-900 and the contribution of all oxidatives to visible light photocatalysis. Moreover, a different influence of TEOA and BQ as scavenger indicates the relatively higher contribution of photoexcited electrons compared to holes, because the oxygen vacancies act as donor [14]. In spite of the enhanced contribution of photoexcited electrons, dominant effect of the hydroxyl radicals ($\cdot OH$) in MB degradation was observed because the superoxide radicals are easily converted to the $\cdot OH$ radicals according to above reaction due to its instability in the aqueous solutions [40,41].

4. Conclusion

In summary, we have demonstrated a simple and versatile one-step synthesis for black TiO_{2-x} microspheres using the USP strategy under an oxygen-deficient environment. XRD patterns, Raman spectra and XPS results revealed that the synthesized black TiO_{2-x} microsphere comprised a higher density of Ti^{3+} and oxygen vacancies.

Photocatalytic experiments that decompose MB under visible light irradiation have demonstrated that black TiO_{2-x} microsphere are 22.1 times more photoactive than white TiO_2 microsphere. This study would present some useful guidelines for a simple one-step synthesis of black metal oxides microspheres with oxygen vacancies for visible-light-driven photocatalysts with a better efficiency.

CRediT authorship contribution statement

Myeongjun Ji: Experiment, Analysis, Investigation, Writing - original draft. **Yong-Ho Choa:** Formal analysis, Writing - original draft, Writing - review & editing. **Young-In Lee:** Project administration, Writing - original draft, Writing - review , & editing, Supervision.

Declaration of Competing Interest

The authors declare that they have no known competing financial interests or personal relationships that could have appeared to influence

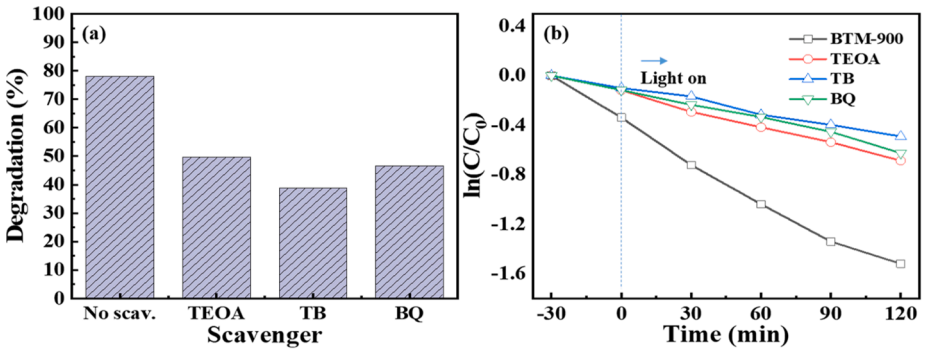

Fig. 5. (a) Degradation efficiency of the photocatalytic degradation of MB using BTM-900 with different radical scavengers, (b) first-order linear transformation ln $(C/C_0) = -kt$ from the kinetic profiles.

the work reported in this paper.

Acknowledgements

This research was supported by the Basic Science Research Program through the National Research Foundation of Korea (NRF) funded by the Ministry of Science, ICT, and Future Planning (NRF-2018R1D1A1B07048149).

Appendix A. Supplementary data

Supplementary data to this article can be found online at https://doi.org/10.1016/j.ultsonch.2021.105557.

References

[1] O. Legrini, E. Oliveros, A.M. Braun, Photochemical processes for water treatment, Chem. Rev. 93 (1993) 671–698.
[2] C.A. Martínez-Huitle, E. Brillas, Decontamination of wastewaters containing synthetic organic dyes by electrochemical methods: A general review, Appl. Catal., B: Environ. 87 (2009) 105–145.
[3] J. Wen, J. Xie, X. Chen, X. Li, A review on g-C_3N_4-based photocatalysts, Appl. Surf. Sci. 391 (2017) 72–123.
[4] I.K. Konstantinou, T.A. Albanis, TiO_2-assisted photocatalytic degradation of azo dyes in aqueous solution: kinetic and mechanistic investigations: A review, Appl. Catal., B: Environ. 49 (2004) 1–14.
[5] X. Chen, S.S. Mao, Titanium dioxide nanomaterials: synthesis, properties, modifications, and applications, Chem. Rev. 107 (2007) 2891–2959.
[6] M.A. Henderson, A surface science perspective on TiO_2 photocatalysis, Surf. Sci. Rep. 66 (2011) 185–297.
[7] M. Sachs, E. Pastor, A. Kafizas, J.R. Durrant, Evaluation of surface state mediated charge recombination in anatase and rutile TiO_2, J. Phys. Chem. Lett. 7 (2016) 3742–3746.
[8] G. Fazio, L. Ferrighi, C.D. Valentin, Photoexcited carriers recombination and trapping in spherical vs faceted TiO_2 nanoparticles, Nano Energy 27 (2016) 673–689.
[9] Y. Liu, Z. Wang, W. Huang, Influences of TiO_2 phase structures on the structures and photocatalytic hydrogen production of CuO_x/TiO_2 photocatalysts, Appl. Surf. Sci. 389 (2016) 760–767.
[10] X. Chen, L. Liu, P.Y. Yu, S.S. Mao, Increasing solar absorption for photocatalysis with black hydrogenated titanium dioxide nanocrystals, Science 331 (2011) 746–750.
[11] A. Naldoni, M. Allieta, S. Santangelo, M. Marelli, F. Fabbri, S. Cappelli, C. L. Bianchi, R. Psaro, V.D. Santo, Effect of nature and location of defects on bandgap narrowing in black TiO_2 nanoparticles, J. Am. Chem. Soc. 134 (2012) 7600–7603.
[12] T. Wang, W. Li, D. Xu, X. Wu, L. Cao, J. Meng, A novel and facile synthesis of black TiO_2 with improved visible-light photocatalytic H_2 generation: Impact of surface modification with CTAB on morphology, structure and property, Appl. Surf. Sci. 389 (2017) 325–332.
[13] A. Naldoni, M. Altomare, G. Zoppellaro, N. Liu, S. Kment, R. Zboril, P. Schmuki, Photocatalysis with reduced TiO_2: from black TiO_2 to cocatalyst-free hydrogen production, ACS Catal. 9 (2019) 345–364.
[14] T.S. Rajaraman, S.P. Parikh, V.G. Gandhi, Black TiO_2: A review of its properties and conflicting trends, Chem. Eng. J. 389 (2020), 123918.
[15] Z. Wang, C. Yang, T. Lin, H. Yin, P. Chen, D. Wan, F. Xu, F. Huang, J. Lin, X. Xie, M. Jiang, Visible-light photocatalytic, solar thermal and photoelectrochemical properties of aluminium-reduced black titania, Energy Environ. Sci. 6 (2013) 3007–3014.
[16] N. Liu, V. Häublein, X. Zhou, U. Venkatesan, M. Hartmann, M. Mackovic, T. Nakajima, E. Spiecker, A. Osvet, L. Frey, "Black" TiO_2 nanotubes formed by high-energy proton implantation show noble-metal-co-catalyst free photocatalytic H_2-evolution, Nano Lett. 15 (2015) 6815–6820.
[17] S.G. Ullattil, P. Periyat, A 'one pot' gel combustion strategy towards Ti^{3+} self-doped 'black' anatase TiO_{2-x} solar photocatalyst, J. Mater. Chem. A 4 (2016) 5854–5858.
[18] V.G. Courtecuisse, K. Chhor, J.-F. Bocquet, C. Pommier, Kinetics of the Titanium isopropoxide decomposition in supercritical isopropyl alcohol, Ind. Eng. Chem. Res. 35 (1996) 2539–2545.
[19] F. Tian, Y. Zhang, J. Zhang, C. Pan, Raman spectroscopy: a new approach to measure the percentage of anatase TiO_2 exposed (001) facets, J. Phys. Chem. C 116 (2012) 7515–7519.
[20] G. Zhu, T. Lin, X. Lü, W. Zhao, C. Yang, Z. Wang, H. Yin, Z. Liu, F. Huang, J. Lin, Black brookite titania with high solar absorption and excellent photocatalytic performance, J. Mater. Chem. A 1 (2013) 9650–9653.
[21] U. Diebold, The surface science of titanium dioxide, Surf. Sci. Rep. 48 (2003) 53–229.
[22] J. Qiu, G. Zeng, M. Ge, S. Arab, M. Mecklenburg, B. Hou, C. Shen, A.V. Benderskii, S.B. Cronin, Correlation of Ti^{3+} states with photocatalytic enhancement in TiO_2-passivated p-GaAs, J. Catal. 337 (2016) 133–137.
[23] C. Rath, P. Mohanty, A.C. Pandey, N.C. Mishra, Oxygen vacancy induced structural phase transformation in TiO_2 nanoparticles, J. Phys. D Appl. Phys. 42 (2009), 205101.
[24] Y. Gao, Y. Masuda, K. Koumoto, Light-excited superhydrophilicity of amorphous TiO_2 Thin Films deposited in an aqueous peroxotitanate solution, Langmuir 20 (2004) 3188–3194.
[25] S. Bai, N. Zhang, C. Gao, Y. Xiong, Defect engineering in photocatalytic materials, Nano Energy 53 (2018) 296–336.
[26] H. Song, C. Li, Z. Lou, Z. Ye, L. Zhu, Effective formation of oxygen vacancies in black TiO_2 nanostructures with efficient solar-driven water splitting, ACS Sustain. Chem. Eng. 5 (2017) 8982–8987.
[27] Q. Zhu, Y. Peng, L. Lin, C.M. Fan, G.Q. Gao, R.X. Wang, A.W. Xu, Stable blue TiO_{2-x} nanoparticles for efficient visible light photocatalysts, J. Mater. Chem. A 2 (2014) 4429–4437.
[28] H. Tan, Z. Zhao, M. Niu, C. Mao, D. Cao, D. Cheng, P. Feng, Z. Sun, A facile and versatile method for preparation of colored TiO_2 with enhanced solar-driven photocatalytic activity, Nanoscale 6 (2014) 10216–10223.
[29] L. Han, B. Su, G. Liu, Z. Ma, X. An, Synthesis of oxygen vacancy-rich black TiO_2 nanoparticles and the visible light photocatalytic performance, Mol. Catal. 456 (2018) 96–101.
[30] J. Leitner, D. Sedmidubsky, Modification of Butler equation for nanoparticles, Appl. Surf. Sci. 525 (2020), 146498.
[31] A.A. Valeeva, E.A. Kozlova, A.S. Vokhmintsev, R.V. Kamalov, I.B. Dorosheva, A. A. Saraev, I.A. Weinstein, A.A. Rempel, Nonstoichiometric titanium dioxide nanotubes with enhanced catalytical activity under visible light, Sci. Rep. 8 (2018) 1–10.
[32] A. Razzaq, A. Sinhamahapatra, T.-H. Kang, C.A. Grimes, J.-S. Yu, S.-I. In, Efficient solar light photoreduction of CO_2 to hydrocarbon fuel via magnesiothermally reduced TiO_2 photocatalyst, Appl. Catal. B 215 (2017) 28–35.
[33] F. Qi, Z. Yang, J. Zhang, Y. Wang, Q. Qiu, H. Li, Interfacial reaction-induced defect engineering: enhanced visible and near-infrared absorption of wide band gap metal oxides with abundant oxygen vacancies, ACS Appl. Mater. Interfaces 12 (2020) 55417–55425.
[34] D. Wan, W. Li, G. Wang, K. Chen, L. Lu, Q. Hu, Adsorption and heterogeneous degradation of rhodamine B on the surface of magnetic bentonite material, Appl. Surf. Sci. 349 (2015) 988–996.
[35] S. Chen, Y. Xiao, Y. Wang, Z. Hu, H. Zhao, W. Xie, A facile approach to prepare black TiO_2 with oxygen vacancy for enhancing photocatalytic activity, Nanomaterials 8 (2018) 245.
[36] X. Xin, T. Xu, J. Yin, L. Wang, C. Wang, Management on the location and concentration of Ti^{3+} in anatase TiO_2 for defects-induced visible-light photocatalysis, Appl. Catal. B 176 (2015) 354–362.
[37] J. Lee, Z. Li, L. Zhu, S. Xie, X. Cui, Ti^{3+} self-doped TiO_2 via facile catalytic reduction over $Al(acac)_3$ with enhanced photoelectrochemical and photocatalytic activities, Appl. Catal. B 224 (2018) 715–724.

[38] K. Nakata, A. Fujishima, TiO_2 photocatalysis: Design and applications, J. Photochem. Photobiol. C 13 (2012) 169–189.
[39] Y. Nosaka, A.Y. Nosaka, Generation and detection of reactive oxygen species in photocatalysis, Chem. Rev. 117 (2017) 11302–11336.
[40] W. Kim, T. Tachikawa, G.-H. Moon, T. Majima, W. Choi, Molecular-level understanding of the photocatalytic activity difference between anatase and rutile nanoparticles, Angew. Chem. 126 (2014) 14260–14265.
[41] G. Rajender, J. Kumar, P.K. Giri, Interfacial charge transfer in oxygen deficient TiO_2-graphene quantum dot hybrid and its influence on the enhanced visible light photocatalysis, Appl. Catal. B 224 (2018) 960–972.